Science Advances
AAAS

advances.sciencemag.org/cgi/content/full/4/8/eaas9459/DC1

Supplementary Materials for

Toward digitally controlled catalyst architectures: Hierarchical nanoporous gold via 3D printing

Cheng Zhu, Zhen Qi, Victor A. Beck, Mathilde Luneau, Judith Lattimer, Wen Chen, Marcus A. Worsley, Jianchao Ye, Eric B. Duoss, Christopher M. Spadaccini, Cynthia M. Friend, Juergen Biener*

*Corresponding author. Email: biener2@llnl.gov

Published 31 August 2018, *Sci. Adv.* **4**, eaas9459 (2018)
DOI: 10.1126/sciadv.aas9459

The PDF file includes:

Other Supplementary Material for this manuscript includes the following:

(available at advances.sciencemag.org/cgi/content/full/4/8/eaas9459/DC1)

Supplementary Materials

Rheological behavior of Ag-Au composite inks

The viscosity of Ag and Au clays is too high for direct mixing and blending. Diluting the clays with a solvent (Melaleuca alternifolia (tea tree) leaf oil, PasteMaker, Sherri Haab) enables mixing and formulation of Ag-Au composite inks with homogeneous, gel-like behavior that exhibit excellent printability and few defects during drying and sintering. Control of thixotropic properties is important for reliable flow through microscale nozzles and careful programming of shear-reversible viscoelasticity is vital for self-supporting shape retention after deposition. The properties were adjusted by altering the solvent content of the composite ink. Fig. S1A shows the apparent viscosity of two Ag-Au inks with 7.6 and 13 weight (wt) % polymer content as a function of shear rate, revealing shear-thinning, non-Newtonian behavior. Fig. S1B compares the corresponding storage and loss moduli as a function of shear stress. The increase in the solvent concentration from 7.6 wt % to 13 wt % results in an order-of-magnitude decrease in the ink apparent viscosity, which improves mixing and printability. For viscoelastic behavior, the ink with 7.6 wt % solvent exhibits an elastic modulus (G') plateau value above 10^5 Pa and a yield stress (τ_y) of ~200 Pa, while the ink with 13 wt % solvent exhibits a plateau value of G' below 10^4 Pa and a τ_y of ~50 Pa. We used Ag-Au inks with 13 wt% solvent for creation of 3D printed hierarchical nanoporous gold (3DP-hnp-Au). The key rheological parameters for our inks are in good agreement with those reported for other colloidal inks designed for this 3D printing technique (*40*). We observed the Ag-Au inks to be highly stable—they can be stored at room temperature for weeks without any degradation in printability.

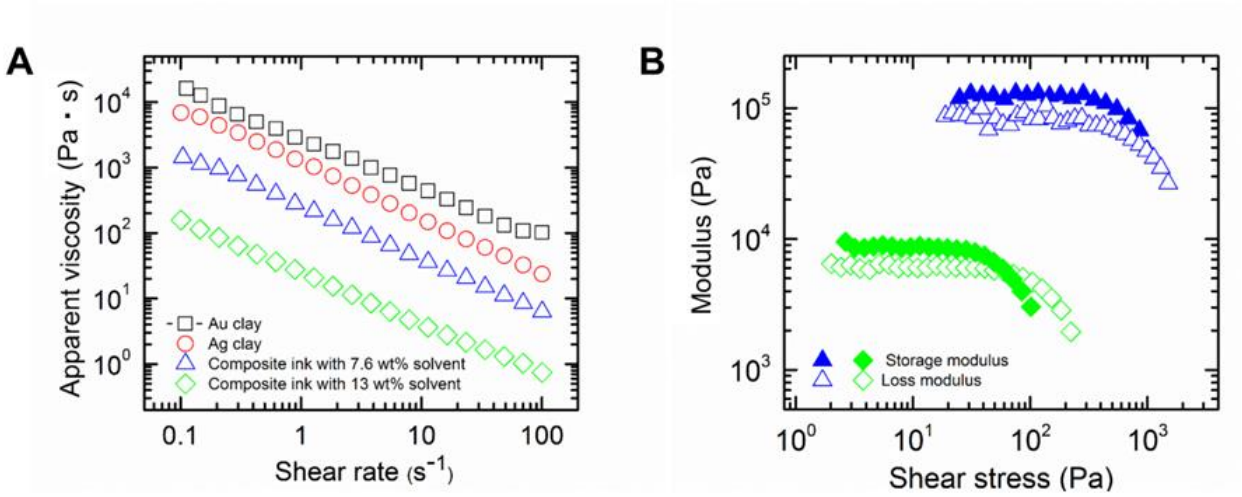

Fig. S1. Rheology of the Ag and Au starting materials and composite inks. (**A**) Logarithmic plot of apparent viscosity as a function of shear rate of as-received Au (unfilled black squares) and Ag clays (unfilled red circles) and as-prepared composite Au-Ag inks with solvent concentrations of 7.6 wt % (unfilled blue triangles) and 13 wt % (unfilled green diamonds). (**B**) Logarithmic plot of storage modulus (filled markers) and loss modulus (unfilled markers) as a function of shear stress of composite inks with 7.6 wt % solvent (blue triangles) and 13 wt % solvent (green diamonds).

Pressure drop simulations

The pressure drop through a porous medium such as nanoporous gold (np-Au) is most appropriately described by Darcy's Law (*41*)

$$(-\Delta P)/L = \mu v/k \qquad (1)$$

where L is the length of the sample, μ is the liquid viscosity, and v is the superficial velocity through the test sample. The permeability, k, is controlled by the pore geometry and is difficult to calculate a priori. It can be roughly estimated using empirical correlations like the Kozeny-Carman equation, initially developed for packed spherical beds; for more elongated geometries one can use the Davies correlation for packed fibers (*42*)

$$k = a^2/(16\alpha^{(3/2)}\ (1+56\alpha^3)) \tag{2}$$

where a is the fiber radius and α is the medium's solid volume fraction (i.e., 1 minus the porosity). The porosity of np-Au is 70%. Using an effective radius of a = 50 nm, both correlations yield permeability values below 10-16 m^2 which even at the lowest flow rates used in this study would yield pressures in excess of 1000 psi, far above the detection limits of our experiments. Given the large flow resistance of np-Au, the hydrodynamics through the 3DP-hnp-Au sample are appropriately modeled as flow through an array of square ducts of width w. The flow rates in our study yield Reynolds numbers, $Re = \rho v w/\mu$ = 5-20 < 2000 (ρ is the density of water), and we thus rule-out turbulence in the duct as a source of pressure loss (*40*). The pressure drop associated with laminar flow in a square duct is provided by the modified Hagen-Poiseuille equation (*43*)

$$\Delta P = 28.45\mu L Q/w^4 \tag{3}$$

where Q is the flow rate through a single square duct. At the exit of the square duct, slumping during the printing process can lead to the formation of a small orifice (Fig. 1E). The finite Re in our system will lead to an inertial pressure loss associated with liquid jetting through the orifice

$$\Delta P = (\rho Q^2)/(2C_0^{\ 2})\ (1/w^4 - 1/d^4) \tag{4}$$

The discharge coefficient, C_0, is usually determined through correlation and depends on both the flow rate and the channel and orifice geometry. Typical values vary from 0.2 to 0.9. More accurate determination of C_0 can be attained by performing laminar flow simulations of the incompressible Navier-Stokes equations in a square duct with a small orifice. The total pressure drop in a square duct is the sum of the laminar pressure drop and the orifice pressure drop. The lattice represents several square ducts in parallel. If all ducts are geometrical equivalent, then the pressure drop in the lattice is equivalent to the drop in a single duct. However, due to variation in the lattice, appropriate hydrodynamic averages for parameters need to be used. This is analogous to the effective resistances of, for example, electrical resistors in parallel.

We use the computational fluid dynamics package STAR-CCM+ 12.02.010 (Siemens) to simulate the laminar, incompressible, 3D Navier-Stokes equation in a square duct with a small orifice. The domain was first separated along two symmetry planes to form a quadrant of the channel and then meshed using the STARC-CCM+ trimmer meshing tool to generate a predominantly hexahedral mesh. Computations were performed on two different meshes, a coarse mesh with typical element size of 2 μm (1.1M cells) and a finer mesh with an element size of 1 μm (3.5M cells). The pressure drop calculation results on the two meshes varied by less than 1%.

A typical simulation result and the flow domain are pictured in fig. S4. In our calculations we varied the flow rate into the square duct from 0.00130 – 0.00781 $ml \cdot s^{-1}$ to correspond with experimental conditions for flow rate through the full sample. Fixed, uniform velocity boundary conditions were applied at the inlet, no-slip conditions were applied at all walls, the two symmetry planes were ascribed symmetry boundary conditions, and a zero pressure boundary condition was applied at the outlet. The pressure drop across the orifice was determined by

calculating the average pressure in planes orthogonal to the flow axis one orifice width, *w*, in both the upstream and downstream directions. We used the segregated solver to search for a steady solution to the flow problem, and terminated the simulation after the residuals stabilized, mass conservation was satisfied to within 10^{-7} %, and the pressure drop stabilized. Typical simulation time on two Intel 8-core Xeon E5-2670 2.6 GHz processors was 10 min.

In fig. S5, we compare the pressure drops from the analytical expression in equations S3 and S4 to the CFD calculations and the experimental data. We see immediately that the laminar pressure drop through the 3 mm long tube is too low to account for the observed pressure drop in the lattice system. We conclude that the pressure drop in the system is dominated by the inertial loss associated with jetting through the orifice. CFD calculations with orifice diameter d = 64 μm yield pressures that are in good agreement with the experimental data. We can also use the CFD results and equation S4 to determine C_0 at each flow rate. This parameter varied from 0.56-0.70 across the flow rates studied, but for simplicity we chose a constant value and set it equal to the average value across the simulations, C_0 = 0.65.

We have simplified the problem by focusing on the pressure drops through a single square duct, and we find that an exit orifice of d = 64 μm yields good agreement with the experimental data. However, the pressure drop through the lattice is a result of the parallel resistance to flow through all of the square ducts which compose the lattice. We thus interpret our choice of d as a hydrodynamically averaged exit orifice similar to the “effective resistance” of resistors in parallel in electrical circuits. Equivalently, the lattice system behaves as an ideal lattice where all of the exit orifices widths are equal to d = 64 μm. From Fig. 1E of the main text we see that d = 64 μm is consistent with the measured physical dimensions in the lattice system.

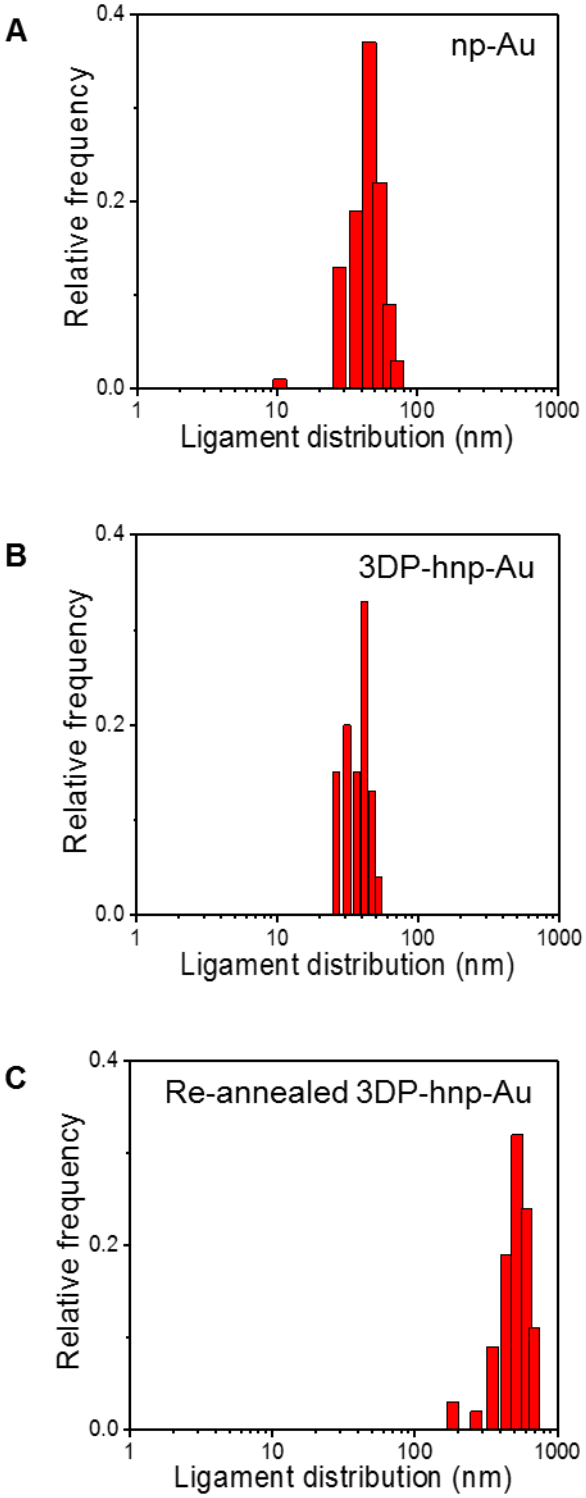

Fig. S2. Ligament size distribution. Histograms of ligament size distributions for (**A**) np-Au, (**B**) 3DP-hnp-Au and (**C**) re-annealed 3DP-hnp-Au (re-annealed at 500 °C for 1h).

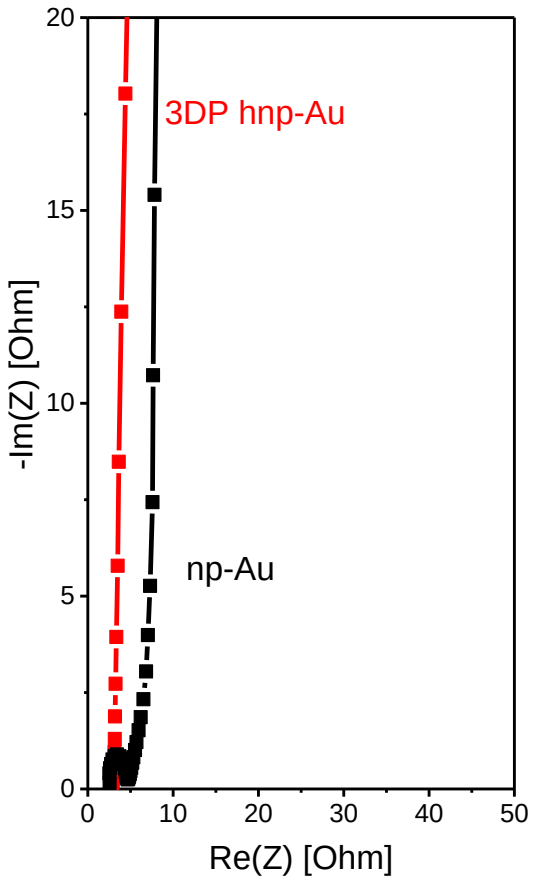

Fig. S3. Nyquist plot of np-Au and 3DP-hnp-Au at open-circuit potential.

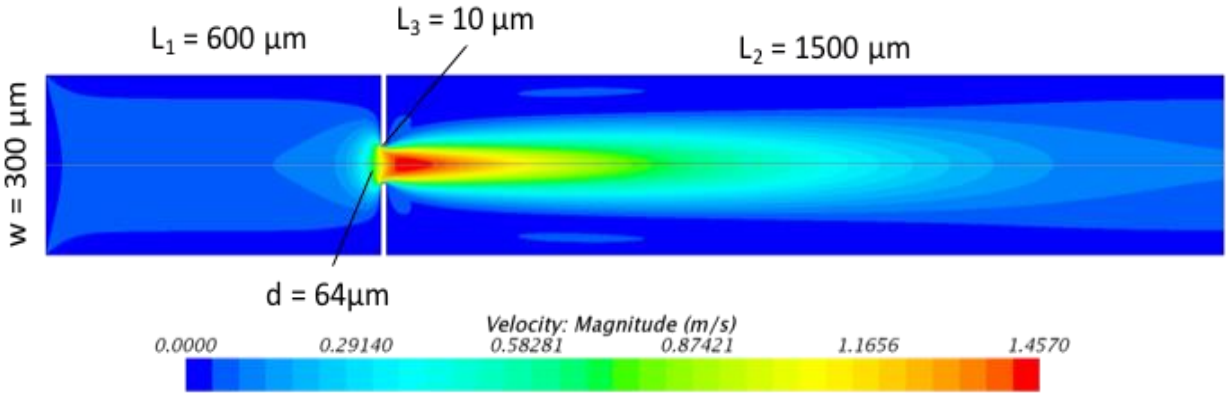

Fig. S4. Computational fluid dynamics (CFD) simulation of the velocity field of a square duct with a square orifice. The flow domain consists of square duct with a square orifice located 600 µm from the duct inlet. The orifice is 10 µm deep and discharges into 1.5 mm long square tube. The magnitude of the velocity field for an inlet flow rate into the lattice of 15mL·min^{-1} is shown. Flow is from left to right and the color mapping indicates the fluid accelerates as it is forced through the orifice.

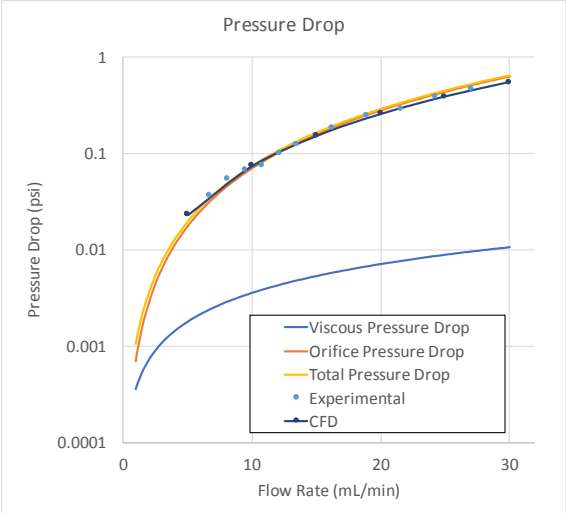

Fig. S5. Pressure drop calculations in the square duct. "Viscous Pressure Drop" is the expected laminar pressure drop through a square channel of width w = 300 µm. "Orifice Pressure Drop" is the calculated pressure drop from equation (*43*). "Total Pressure Drop (100 µm)" is the sum of the laminar and orifice pressure drops. These calculated curves are compared to CFD simulations and experimental data.

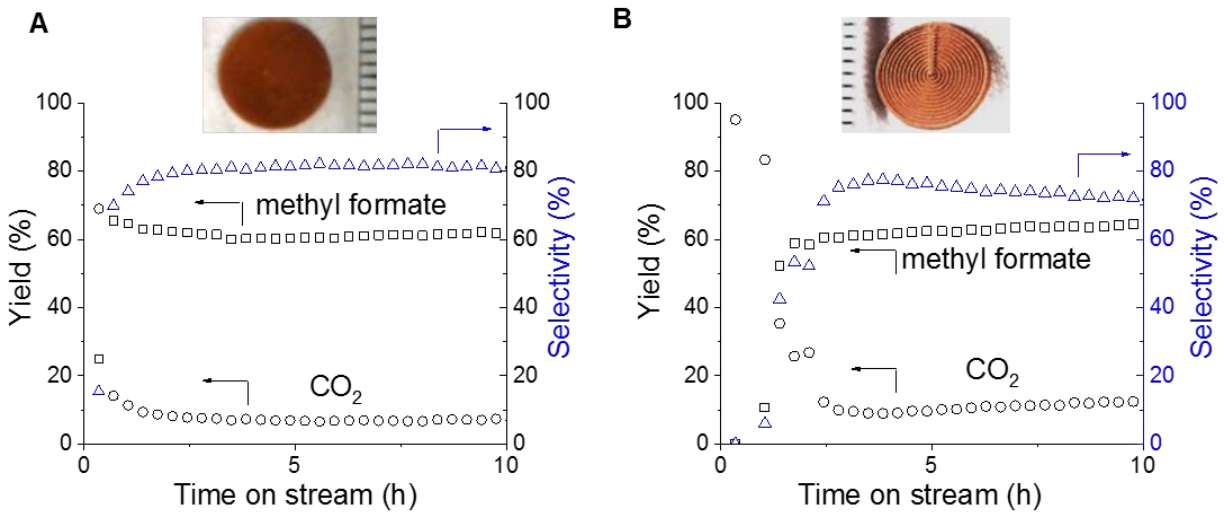

Fig. S6. Methanol oxidation to methyl formate and carbon dioxide at 150°C. Yield and selectivity towards methyl formate versus time of (**A**) np-Au and (**B**) 3DP-hnp-Au (80 mg) catalyst samples with the same nominal thickness. Reaction conditions: 10% Methanol; 20% O_2 in He balance. Insets show optical images of the samples.

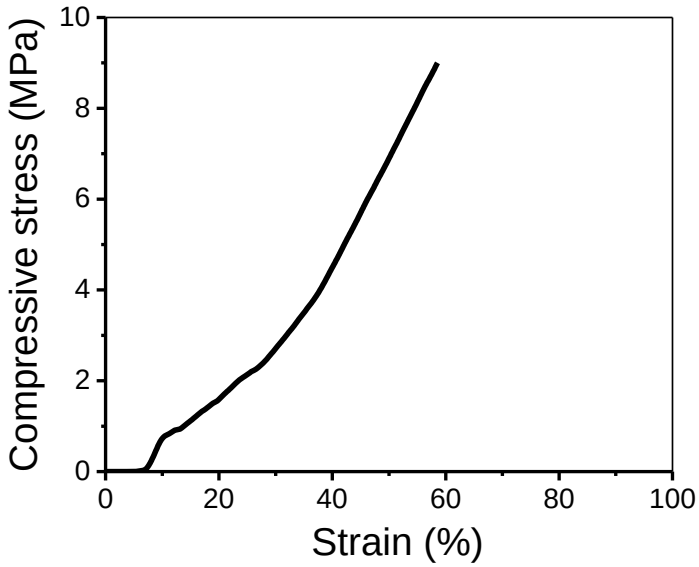

Fig. S7. Compressive stress-strain curve of 3DP-hnp-Au.

Table S1. Methanol oxidation under different reaction conditions for np-Au and 3DP-hnp-Au.

Conditions	npAu_ingot	3DP-hnp-Au
10% CH_3OH	r = 0.016 mmol g^{-1} s^{-1}	r = 0.034 mmol g^{-1} s^{-1}
20% O_2	80% S	71% S
F = 50 mL min^{-1}	72% Conv.	78% Conv.
10% CH_3OH	r = 0.013 mmol g^{-1} s^{-1}	r = 0.028 mmol g^{-1} s^{-1}
5% O_2	90% S	81% S
F = 50 mL min^{-1}	60% Conv.	65% Conv.
10% CH_3OH	r = 0.018 mmol g^{-1} s^{-1}	r = 0.039 mmol g^{-1} s^{-1}
5% O_2	92% S	86% S
F = 75 mL/min	55% Conv.	60% Conv.

Rate of methanol conversion (r), selectivity for methyl formate (S) and total conversion of methanol (Conv.)